THE SPECTRAL ANALYSIS OF AN AERO-ENGINE ASSEMBLY INCORPORATING A SQUEEZE-FILM DAMPER

R. Holmes and M.M. Dede
Department of Mechanical Engineering
University of Southampton
Southampton, England

Aero-engine structures have very low inherent damping and so artificial damping is often introduced by pumping oil into annular gaps between the casings and the outer races of some or all of the rolling-element bearings supporting the rotors.

The thin oil films so formed are called squeeze film dampers and they can be beneficial in reducing rotor vibration due to unbalance and keeping to reasonable limits the forces transmitted to the engine casing. However, squeeze-film dampers are notoriously non-linear and as a result can introduce into the assembly such phenomena as subharmonic oscillations, jumps and combination frequencies.

The purpose of the research described in this paper is to investigate such phenomena both theoretically and experimentally on a test facility reproducing the essential features of a medium-size aero engine.

The forerunner of this work has been published in refs. [1],[2]. It was concerned with the examination of a squeeze-film damper in series with housing flexibility when supporting a rotor. The structure represented to a limited extent the essentials of the projected Rolls Royce RB401 engine. That research demonstrated the ability to calculate the oil-film forces arising from the squeeze film from known motions of the bearing components and showed that the dynamics of a shaft fitted with a squeeze film bearing can be predicted reasonably accurately.

An aero-engine will normally have at least two shafts and so in addition to the excitation forces which are synchronous with the rotation of one shaft, there will also be forces at other frequencies from other shafts operating on the squeeze-film damper. The present paper is concerned with theoretical and experimental work to consider severe loading of squeeze-film dampers and to include these additional effects. The theoretical methods are similar to those discussed in references [1] and [2].

* Now with General Electric Company, Cincinnati, U.S.A.

NOTATION

a	Mass ratio m_{e2}/m_h
b	Linear damping coefficient
c	Radial clearance of the squeeze-film bearing
d	Seal end-gap
D	Diameter of squeeze-film bearing
F	Amplitude of force transmitted to engine frame
k	Stiffness of the flexible bars 6 in Fig. 2
ℓ	Squeeze-film bearing land width
L	Radial depth of sealing ring
L_g	Width of groove
$m_e c\omega_2^2$	Normalising parameter for forces
m	Rotor mass
$m_{e1,2}$	Effective mass of rotor 1,2.
m_h	Effective mass of rotor 1 plus bell housing 4, squeeze-film bearing housing 5 and flexible bars 6 in Fig. 2.
p_{cav}	Cavitation pressure
p_s	Oil supply pressure
$P_{c1,2}$	Unbalance force on rotor 1, 2
R	Radius of the squeeze-film bearing
$r_{1,2}$	Radius of unbalance of mass $m_{1,2}$ from axis of rotation.
T	Transmissibility = force reaching ground ÷ unbalance force
x	Amplitude of rotor vibration
$u_{1,2}$	Effective radius of unbalance of rotor (1,2) mass from axis of rotation
$\bar{W}$	$g/c\omega_n^2$

α	ω_1/ω_2
β_n	$\frac{\mu R}{m_{e2}\omega_n}\left(\frac{\ell}{c}\right)^3$
λ	Boundary-condition factor
ψ	Attitude angle
ε	Eccentricity ratio
μ	Dynamic viscosity
$\mu\omega_n(R/c)^2$	Normalising parameter for pressures
$\omega_{1,2}$	Angular velocity of rotor 1.2.
ω_n	Undamped natural frequency
$'$	Differentiation with respect to ωt

THE TEST FACILITY

Fig. 1 shows diagrammatically a section through the front end of a modern aero-engine, having two nested rotors. The structure is subjected to a variety of forces, for example forces arising from unbalance in the H.P. rotor are transmitted into bearing housings supporting the L.P. rotor, which often incorporate squeeze film dampers. A test facility was designed to reproduce such essential features of the aero-engine assembly, in particular to examine the vibration of a rotor employing a squeeze-film damper, whose housing can be under the influence of an excitation force which is different in frequency from that of its shaft rotation.

A drawing of the test facility is shown in Fig. 2. The assembly consists of two sub-assemblies comprising rotors 1 and 2, representing the aero engine HP and LP shafts respectively. These are capable of being driven at different speeds by variable-speed motors through pin-and-cord couplings. The unbalance mass 3 produces a dynamic force which is transmitted through the bell-housing 4 to the housing of the squeeze-film damper 5, which is itself flexibly supported at 6 and contains the roller bearing 7. The outer race of this bearing is surrounded by the squeeze-film damper 8, which is provided with either R10 oil or Shell calibration fluid. These have viscosities at room temperature of 15cp and 5cp respectively. The unbalance mass 9 provides a further force at the inner race of the roller bearing, whose movement is permitted by the self-aligning bearing 10 and whose location represents a node of rotor 2.

The damper has two bearing lands which are separated by a central circumferential oil-supply groove. End-plates are attached at both ends of the squeeze film to afford some sealing. The axial end clearance between the plates and the dampers and thus the extent of the sealing can be varied by the

insertion of spacing shims. The rotation of the damper journal is prevented by dogs located in one of the end plates, providing sufficient clearance to allow the journal to move in any part of the squeeze-film clearance space. The squeeze-film damper diameter is set by the outer race of the roller bearing 7 (140 mm). The damper land length and its radial clearance are typical of aero engine application (Fig. 3).

The rig parameters

Preliminary impulse tests were carried out to define the total effective stiffness of the flexible bars 6 and to find the effective masses of rotors 1 and 2 at the squeeze-film location. From tests on the flexibly-mounted housing alone, its natural frequency was found to be 192 Hz. Using an effective housing mass of 3.9 kg the total stiffness of the flexible bars was found to be about 5.68×10^6 N/m. With rotor 2 alone in position, the natural frequency was 75 Hz in the horizontal and 71 Hz in the vertical direction. The difference was almost certainly due to the movement of bearing 7 within its squeeze film annulus. This was empty of oil at the time of testing and promoted bouncing of bearing 7, By taking 73 Hz as an averaged frequency, the effective mass of rotor 2 was found to be 22.16 kg. A similar test was carried out with rotor 1 in position and with rotor 2 removed, and finally with both rotors in position. Table 1 shows the findings of all the tests in a concise form.

Table 1

Arrangement	Horizontal (Hz)	Vertical (Hz)	Effective mass (kg)	Accepted Natural Freq. (Hz)
Squeeze film (SF) housing only	192	192	3.9	192
Rotor 2 and SF assembly	75	71	22.2 (rotor 2 only)	73
Rotor 1 and SF assembly	94	103	10.0 (rotor 1 only)	98
Rotors 1 and 2	61.2	63.6	32.4	62

The undamped natural frequency of the complete assembly was taken as 62 Hz (3720 c/min) and it can be seen that the effective mass in the last case is about equal to the sum of those in the previous two cases. The static load

provided by rotor 2 on the squeeze-film was half its weight, corresponding to 50/2 or 25 kg. The dynamic loads arose from the unbalance masses 3 and 9, and can be expressed as $P_{c1} = m_1 r_1 \omega_1^2$ and $P_{c2} = m_2 r_2 \omega_2^2$, where m_1 and m_2 are respectively the unbalance masses on rotors 1 and 2, r_1, r_2 are the radii of the mass locations from the centre of rotation of each shaft, and ω_1 and ω_2 are the speeds of the shafts. However, in the analysis it is more convenient to consider the unbalance mass-radius product to have a magnitude equal to the total effective mass of each rotor at an effective unbalance radius u.

SINGLE-SHAFT VERSION OF THE TEST FACILITY

The test facility was first separated into its two rotor components by removing the bell housing 4. Tests were carried out on the LP rotor (2) alone mounted in the squeeze-film damper to investigate its performance characteristics.

A diagrammatic representation of the test facility in this configuration is given in Fig. 4. The degree of damping offered by the squeeze-film is quite critical. If it is too great the damper operates rather like a rigid link and conveys little benefit to the system. On the other hand if the damping is too small, excessive movements take place in the squeeze film annulus.

Assuming for a moment that the damping is linear, its effect in series combination with the rotor mass and housing flexibility is shown in Figs. 5a, b, c. From these figures it can be seen that there is likely to be an optimum value of damping b to ensure reasonable levels of rotor vibration relative to the engine frame (Fig. 5a), relative to the bearing housing (Fig. 5b) and of transmissibility (Fig. 5c). Complications are introduced by the fact that due to non-linearity of the squeeze-film its damping increases greatly with eccentricity ratio ε. Fig. 5b indicates that high values of ε can arise over a considerable frequency range, particularly at low values of b. Under these conditions the apparent benefits of low damping indicated in Figs. 5a and 5c may not be realised.

The most critical operating condition occurs at a speed corresponding to the natural frequency of the assembly, $\frac{\omega}{\omega_n} \simeq 1$. From Figs. 5a,b,c, three distinctive features can be observed.

a) The non-dimensional amplitude of vibration of the rotor x_2/u <u>increases</u> with non-dimensional damping $b/\sqrt{km}$.

b) The non-dimensional eccentricity of the rotor in the squeeze-film damper, $\varepsilon/(u/c)$, is <u>independent</u> of non-dimensional damping $b/\sqrt{km}$, where $\varepsilon = (x_2 - x_1)/c$.

c) The transmissibility T <u>increases</u> with non-dimensional damping $b/\sqrt{km}$.

Thus the assembly is quite unlike one having a damper in parallel with its flexibility.

Preliminary tests were first run on the reduced test facility to ascertain whether these trends were exhibited in the actual non-linear system. Various means were adopted by which the effective damping could be altered. For example, damping could be increased by

i) increasing the oil viscosity
ii) tightening the sealing, or
iii) increasing the supply pressure.

Figs. 6a, b, c show the results obtained for various sealing conditions, oil viscosities and supply pressures. From these, conclusions can be drawn which are consistent with the three distinctive features using the linear damping model. This model thus provides a reasonable qualitative guide to damper performance in the most critical region of rotor operation.

The next purpose of the reduced test facility was to look for evidence of jump phenomena and sub-harmonic vibrations in the frequency responses as these had been observed in certain engine tests where the oil viscosity was low.

Efforts were therefore made to produce conditions on the test facility, which were likely to be conducive to such jumps. This indeed proved to be possible when the support flexibility was locked out and when the supply pressure to the squeeze-film was at a fairly low level. Fig. 7a shows a sequence of orbits of rotor vibration relative to the squeeze-film damper housing using a supply pressure of 5 psi. At about 3450 rev/min a pronounced jump up was observed. This was almost certainly due to a change in the effective parameters governing system performance. This change was probably brought about by sudden venting of the squeeze film clearance space from atmosphere, resulting in a change of level at which the negative hydrodynamic pressure in the squeeze film was curtailed. Fig. 7a shows a set of pressure recordings which seem to bear this out. This would result in much smaller squeeze-film forces and hence a much larger orbit of vibration of the rotor centre, and can be predicted by numerical computation (Fig. 7b). For the latter purpose, the hydrodynamic squeeze-film forces were numerically derived by integrating the oil-film pressure around the circumference of the damper. These forces depend on the oil-film cavitation model used and on the end-plate clearance expressed as a λ factor [2]. The λ-factor describes the boundary conditions imposed at the ends of the squeeze-film damper by the tightness of the end-seals and in the present research has been extended to cover various $\ell/_D$ ratios (Fig. 7c). In the present case where the $\ell/_D$ ratio is 0.045 a λ-factor of 0.09 was used, being appropriate to an end plate gap/clearance ratio of 0.23 and an end-plate clearance of 0.053 mm. The non-linear equations of motion were then solved by integration at each time step of a marching scheme.

With regard to subharmonic vibrations, Fig. 8a shows a succession of orbits of the LP shaft (2) relative to the squeeze-film housing for a u/c value of 0.33 and using Shell calibration fluid as the lubricant. The speed range covered was 3880 to 5075 rev/min. with the undamped natural frequency at 4300 rev/min (73 Hz). The centre of the LP rotor executed a butterfly type of motion, such that it completed each "wing" for alternate revolutions of the

rotor. This half-engine order motion persisted over a wide range of operational speed. Eventually the "wings" coalesced after the critical speed was passed to produce an essentially single orbit. The predicted orbits for the same speeds are shown in Fig. 8b, in which the same double looping is clearly evident. Coalescing is predicted somewhat later in the speed range than was measured.

Z-MODULATION

The z-mod technique presents a great deal of useful information on the harmonic content of a signal in a very compact way and by this means it is possible to appreciate an overall performance signature of an engine over a wide speed range. A z-mod is similar to a "waterfall" diagram used in rotating machinery diagnostics except that engine speeds are arranged along the x axis, instead of along the y axis, frequency content is displayed along the y axis instead of along the x axis and the strength of a frequency component is represented as a colour (or as a degree of blackness) instead of a laid-back peak.

By way of elucidating this technique, consider Fig. 9a which shows an experimental z-mod of horizontal components of LP rotor vibration relative to the squeeze-film housing using a specially-adapted commercial spectral analyser. It will be observed that half-integer order frequency components manifest themselves strongly around the natural frequency of 73 Hz.

Software was developed to obtain theoretical z-mods with the wide range of colours available on many microcomputers. This made possible direct comparisons of predictions with the experimental z-mods.

The z-mod presentation of numerically-predicted horizontal LP shaft vibration relative to the squeeze-film damper housing is shown in Fig. 9b, and compares well with the experimental z-mod of Fig. 9a. Half engine orders are indeed predicted around 73Hz. This is due to squeeze-film non-linearities manifesting themselves when the overall vibration becomes appreciable, as it does around the natural frequency of 73Hz.

Half-integer orders are a common feature in loose assemblies [3]. It is not unreasonable to suppose that in the present case the squeeze-film damper clearance was acting as a loose assembly on account of the fairly high unbalance load together with the fairly short squeeze-film damper lands and the low viscosity of the oil supplied. When heavier oil was introduced all half-integer order harmonics disappeared.

A non-linear system can be conceived in which a subharmonic may be excited, whose frequency is half that of the excitation frequency. To show that this is possible, consider a system with a square-law restoring force subject to a steady force (such as gravity) and to harmonic excitation (such as that due to unbalance), both of which are provided by the test facility. Let the system satisfy the differential equation,

$$m\ddot{x} + \gamma x + \Omega x^2 = P_0 + P_1 \cos \omega t, \quad \text{say}$$

that is, the effective stiffness of the squeeze film is $\gamma - \Omega x$.

Let us assume that a possible solution is

$$x = A \cos \frac{\omega}{2} t.$$

Thus $$A\left(\gamma - \frac{m\omega^2}{4}\right) \cos \frac{\omega t}{2} + \frac{\Omega A^2}{2} + \frac{\Omega A^2}{2} \cos \omega t = P_o + P_1 \cos \omega t$$

This equation is satisfied for

$$A = \left(\frac{2P_o}{\Omega}\right)^{\frac{1}{2}}$$

$$A = \left(\frac{2P_1}{\Omega}\right)^{\frac{1}{2}}$$

and $$\omega = 2\sqrt{\frac{\gamma}{m}}$$

The first two conditions imply that $P_o = P_1$, which happens to be conducive to rattle since then the gravity force P_o is just neutralised by the dynamic lift-off force P_1. This example shows that a second harmonic, resulting from the non-linear term, can prevail, being compensated by a certain intensity of excitation at some specific frequency. This frequency is illustrated most strikingly when a squeeze-film damper is accompanied by a parallel spring of stiffness γ. In that case ω corresponds to twice the first undamped natural frequency and a subharmonic resonance of order ½ is exhibited [4].

Since both harmonics and subharmonics can occur simultaneously, oscillations having any half integer ratios to the excitation frequency are possible, given the correct form of non linearity. These oscillations are in fact combination frequencies and will be discussed later.

THEORETICAL ANALYSIS FOR COMPLETE CONFIGURATION OF THE TEST FACILITY

The dynamically-equivalent structure of the test facility with both rotors connected is shown in Fig. 10. It may be shown [2] that a set of non-dimensional parameters which describe this non-linear system can be expressed as $\bar{W}$, β_n, $u_{1,2}/c$, a, α, ω_2/ω_n, $p_{cav}/\mu\omega_n(R/c)^2$, and $p_s/\mu\omega_n(R/c)^2$.

The non-linear equations of motion were solved by again integrating at each time step of a marching scheme. To obtain a feel for the kind of results obtained, Fig. 11a shows a typical vibration orbit for the housing of the squeeze-film bearing relative to ground while Fig. 11b shows the vibration

orbit of rotor 2 relative to ground. In Fig. 11c the orbit of rotor vibration relative to the squeeze-film housing is shown. For these cases the following values were applied:

No-end sealing	$\bar{W} = 0.28$	$\alpha = 2.0$
	$\beta_n = 0.016$	$a = 1.5$
	$\mu\omega_n(R/c)^2 = 154.5$ psi	$\omega_2/\omega_n = 0.93$
	$u_1/c = 0.23$	$p_{cav} = -20$ psi
	$u_2/c = 0.23$	$p_s = 20$ psi

By putting $\alpha = -2.0$, counter-rotation of rotor 1 relative to rotor 2 is represented. The resulting orbits for this condition are shown in Fig.12 in the same sequence as for Fig. 11. The same cases were then treated with end-plates included (Fig.13). These last orbits indicate a much more stable system and steady states are achieved much more quickly, due to the higher damping ensured by the end plates.

COMPARISON OF NUMERICAL ORBITS AND EXPERIMENTAL OBSERVATIONS FOR COMPLETE CONFIGURATION OF THE TEST FACILITY

Fig.14 shows a specimen set of comparisons of rotor 2 vibration orbits relative to the ground, when rotating at 3000 rev/min with rotor 1 stationary. For these comparisons the full non-linear equations were solved again using the λ-factor approach developed in ref.[2]. Fig. 14 is for a case of fairly tight sealing ($\lambda = 0.0356$) and the agreement between experimental and predicted orbits of vibration is seen to be reasonable, the scale factors used for each set of orbits being the same. This agreement is representative of comparisons over a wide range of speeds, oil viscosities, supply pressures and unbalances and a cavitation pressure of -20 psi has been used throughout.

Consider now cases in which rotors 1 and 2 rotate in first co-rotation and then counter-rotation relative to each other. Detailed comparisons between predicted and experimental orbits are not appropriate here due to the indeterminacy of the phasing between shafts 1 and 2 arising from slight drifts in speed. However it is possible to observe certain distinctive features from comparisons of experimental orbits of rotor vibration relative to ground for the co-rotating and counter-rotating cases. The same distinctive features can then be sought in the comparison of the numerically-predicted orbits.

Some experimental orbits are shown in Figs. 15 and 16 (upper) for $\omega_1/\omega_2 = \pm 1.3$. The most distinctive differences are observed to be the rounded nature of the orbits for the co-rotating cases as opposed to the spiky nature for the counter-rotating. The same features can be observed in the numerically-predicted orbits, Fig.15 and 16 (lower). In addition, there is broad agreement on orbit size.

It was noticeable during running that the test facility was much more noisy for counter rotation, suggesting that transmitted forces were higher, perhaps due to the more sudden reversals in the orbits.

FREQUENCY CONTENT OF SYSTEM VIBRATION WHEN SHAFTS ARE IN CO-ROTATION AND IN COUNTER-ROTATION : COMBINATION FREQUENCIES

In a linear system resonance occurs when the system is excited by a harmonic force of frequency near to the undamped natural frequency of the system. In a non-linear system other kinds of resonance are possible.

Consider a non-linear system subject to an excitation consisting of two harmonic components as we have in this test facility. Thus,

$$m\ddot{x} + f(x) = P_1 \cos(\omega_1 t + \phi_1) + P_2 \cos(\omega_2 t + \phi_2)$$

in which we can expand f(x) in the form of a Taylor series,

$$f(x) = a_1 x + a_2 x^2 + a_3 x^3 + \ldots$$

Now assume that x is roughly harmonic, that is

$$x = X_1 \cos \omega_1 t + X_2 \cos \omega_2 t$$

Thus f(x) will consist of terms in

$$\cos \omega_{1,2} t$$

$$\cos^2 \omega_{1,2} t = \tfrac{1}{2}(1 + \cos 2\omega_{1,2} t)$$

$$\cos^3 \omega_{1,2} t = \tfrac{1}{4}[3 \cos \omega_{1,2} + \cos 3\omega_{1,2} t]$$

$$\cos \omega_1 t \cos \omega_2 t = \tfrac{1}{2} \cos(\omega_1 + \omega_2)t + \tfrac{1}{2} \cos(\omega_1 - \omega_2)t$$

$$\cos 2\omega_1 t \cos \omega_2 t = \tfrac{1}{2} \cos(2\omega_1 + \omega_2)t + \tfrac{1}{2} \cos(2\omega_1 - \omega_2)t \text{ etc.}$$

All possible linear combinations of the two frequencies ω_1 and ω_2 thus appear and in general it can be said that the solution will contain the frequencies

$$n\omega_1$$

$$m\omega_2$$

and $$n\omega_1 \pm m\omega_2$$

where m and n are whole numbers, the latter being known as combination oscillations. They also manifested themselves in half-integer orders during tests on the single-shaft version of the test facility (Fig. 9).

Fig. 17 shows experimental z-mods for cases of co-rotation and counter-rotation in which $\omega_1/\omega_2 = \pm 1.3$. These relate to vertical vibration of the squeeze-film housing relative to ground. Many LP and HP engine orders are

present in both, as are probable combination frequencies. By taking a vertical section of the z-mod at L.P. rotor speeds of say 40, 60 and 75 rev/s, frequency spectra can be constructed. Figs. 18a, b show such spectra for co-rotation and counter-rotation respectively. Some suggestions are made on Fig. 18 as to what these frequencies might be in terms of HP and LP rotor speeds.

CONCLUSIONS

The purpose of the research described in this paper has been to reproduce on a test facility phenomena exhibited in aero-engine tests. These included subharmonic oscillations, jumps in frequency response and combination frequencies. All of these effects were reproduced and could be predicted by numerical computation or by appreciation of non-linear mechanics. Furthermore, at speeds in the vicinity of the undamped natural frequency, a linear treatment gave a sound understanding of trends in vibration performance.

A method was presented by which the above features could be appreciated in a comprehensive way. This is known as the z-modulation technique and utilises up-to-date computer graphics facilities.

REFERENCES

[1] Holmes, R. and Dogan, M. 'Investigation of a rotor bearing assembly incorporating a squeeze film damper bearing.' Proc. Instn. Mech. Engrs. vol. 24, No. 3, 1982.

[2] Holmes, R and Dogan, M. 'The performance of a sealed squeeze-film bearing in a flexible support structure.' Proc. Instn. Mech. Engrs. vol. 199, No. C1, 1985.

[3] Angelo, M. 'Vibration Monitoring of Machines. Brüel nd Kjoer Technical Review No. 1 1987, pp.5,6.

[4] Nikolajsen, J.L. and Holmes, R. 'Investigation of squeeze-film isolator for the vibration control of a flexible rotor.' Proc. Instn. Mech. Engrs. vol. 21, No. 4, 1979.

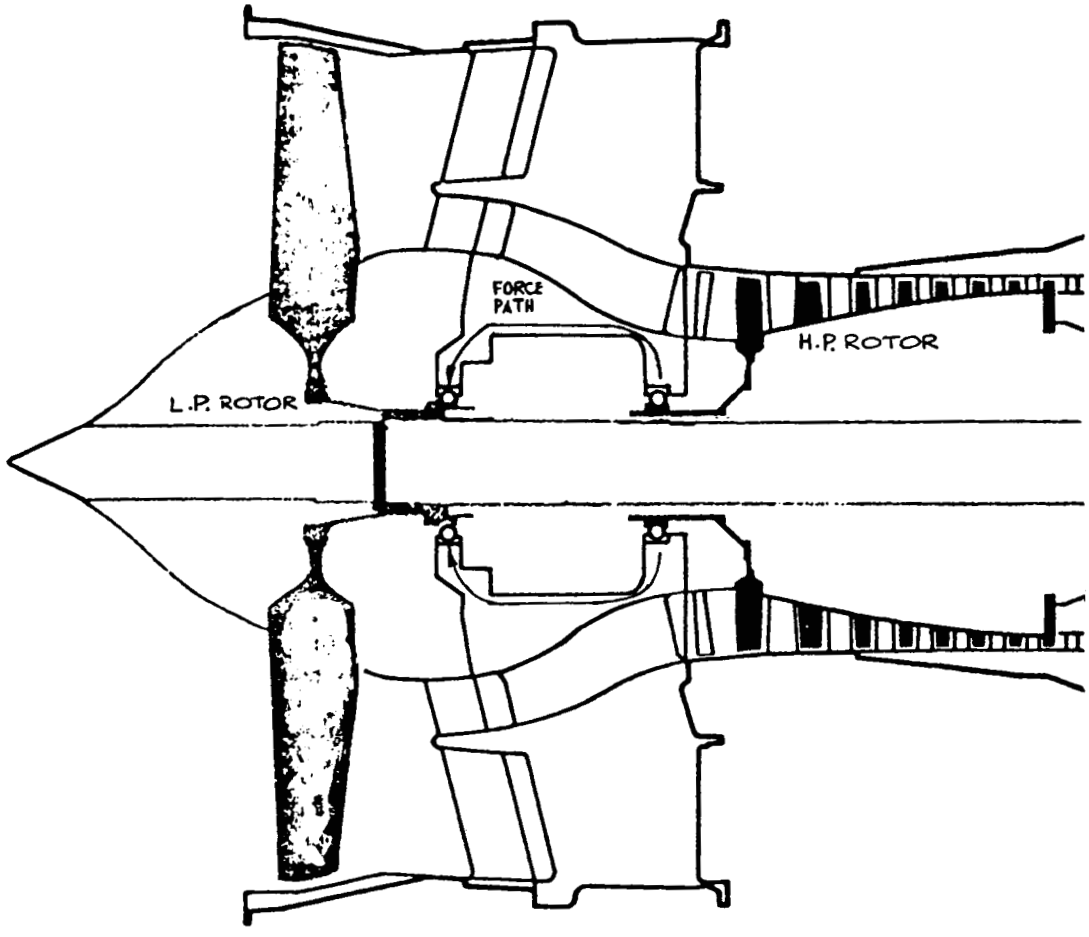

Fig. 1 : Diagrammatic section through aero-engine front end.

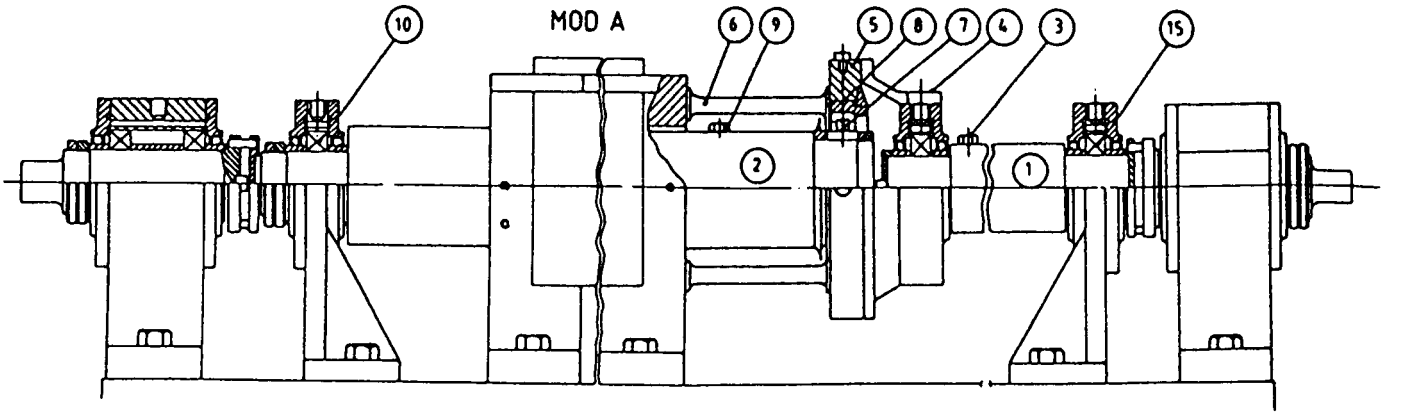

Fig. 2 : Experimental test facility.

1 Rotor 1
2 Rotor 2
3 Unbalance mass
4 Bell housing
5 Squeeze - film housing
6 Flexible bars
7 Roller bearing
8 Squeeze - film damper
9 Unbalance mass
10 Self - aligning bearing

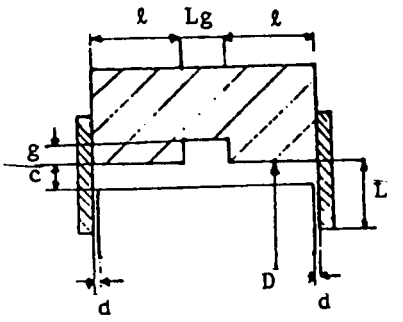

c = 0.23 mm
d = 0.076 mm
D = 140 mm
g = 0.63 mm
ℓ = 6.26 mm
Lg = 7.00 mm
L = 7.76 mm

Fig. 3 : Damper geometry.

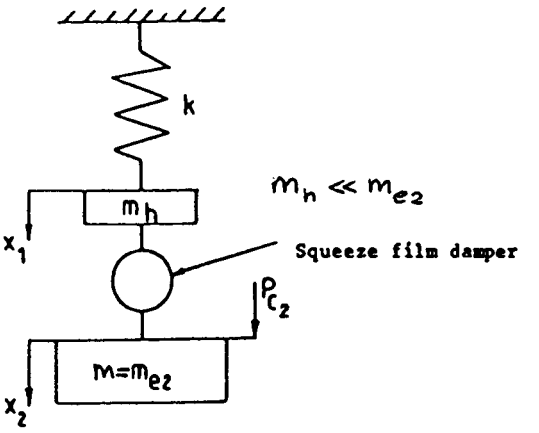

Fig. 4 - Mathematical model of the rig.

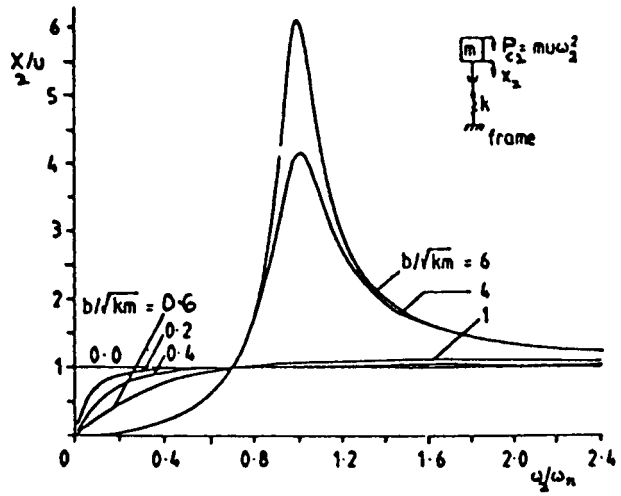

Fig. 5a - Amplitude of rotor vibration relative to engine frame.

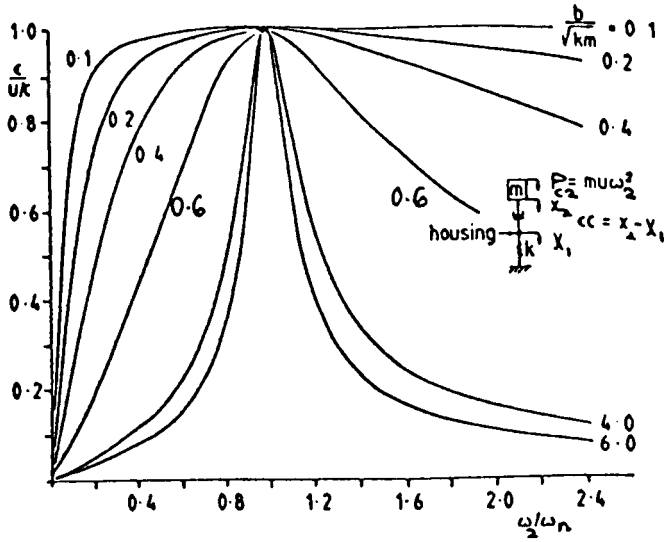

Fig. 5b - Amplitude of rotor vibration relative to damper housing.

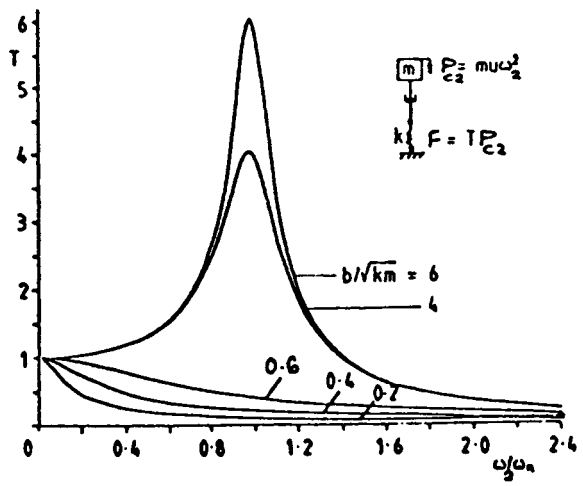

Fig. 5c - Transmissibility.

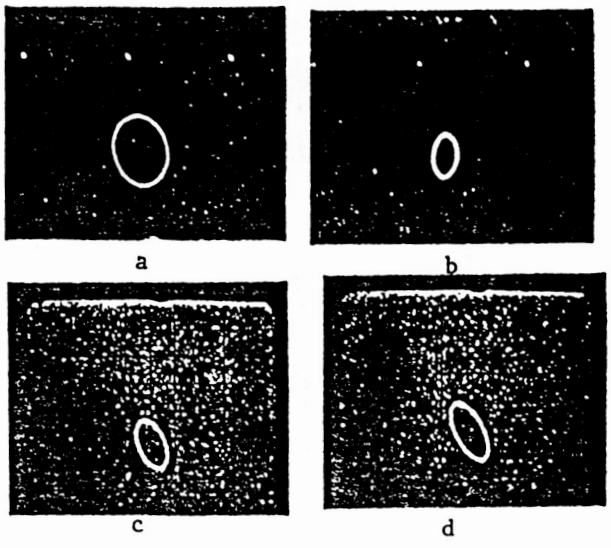

Rotor vibration relative to engine frame

Fig. 6 : Experimental orbits.

$\frac{\omega_2}{\omega_n} = 1, \frac{u}{c} = 0.23$

a) sealing tight
viscosity high
supply pressure low

b) sealing loose
viscosity high
supply pressure low

c) sealing tight
viscosity low
supply pressure low

d) sealing tight
viscosity low
supply pressure high

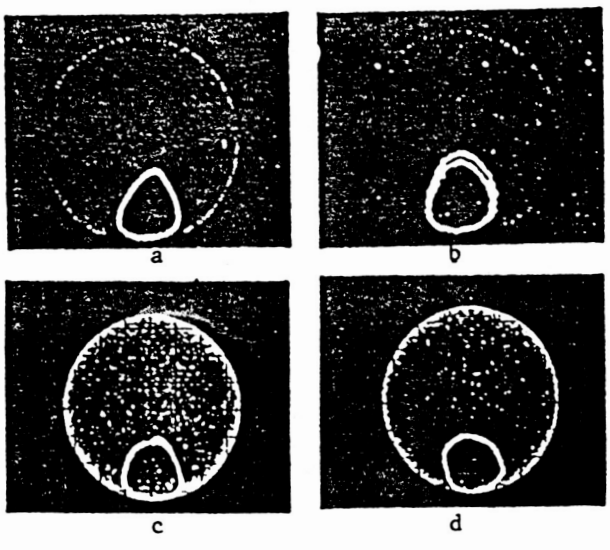

Rotor vibration relative to the bearing housing

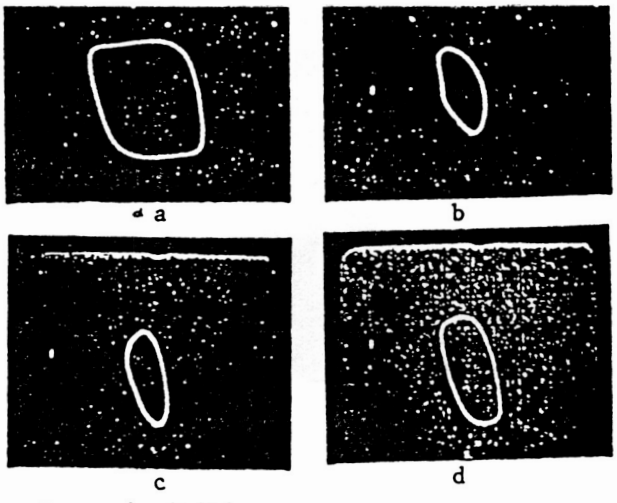

Transmissibility

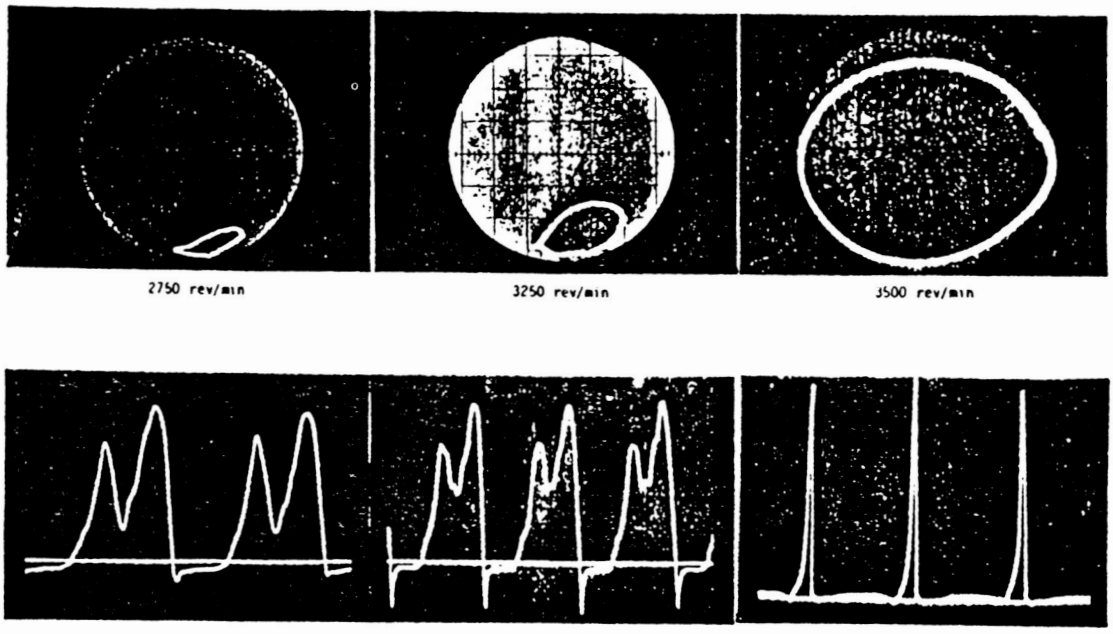

Fig. 7 : (a) Experimental orbits and pressure recordings (1 cm = 200 psi), u/c = 1.055.

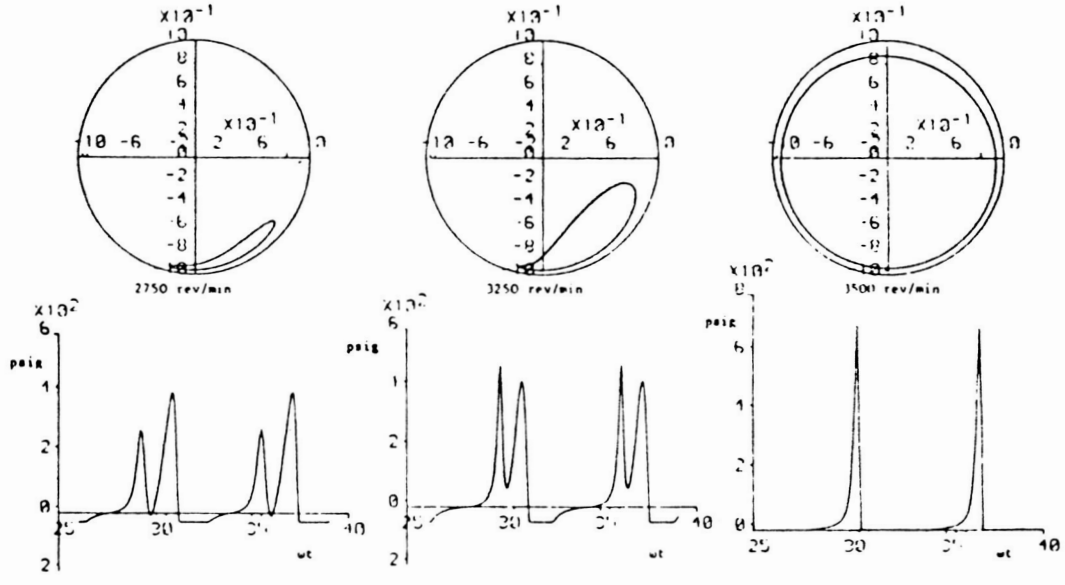

Fig. 7 : (b) Numerical orbits and pressures, u/c = 1.055.

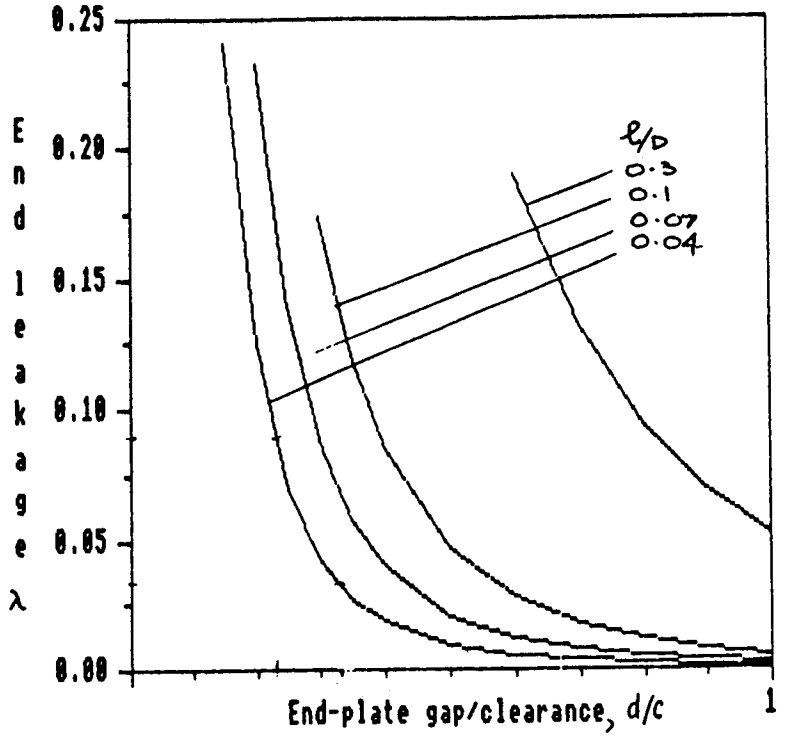

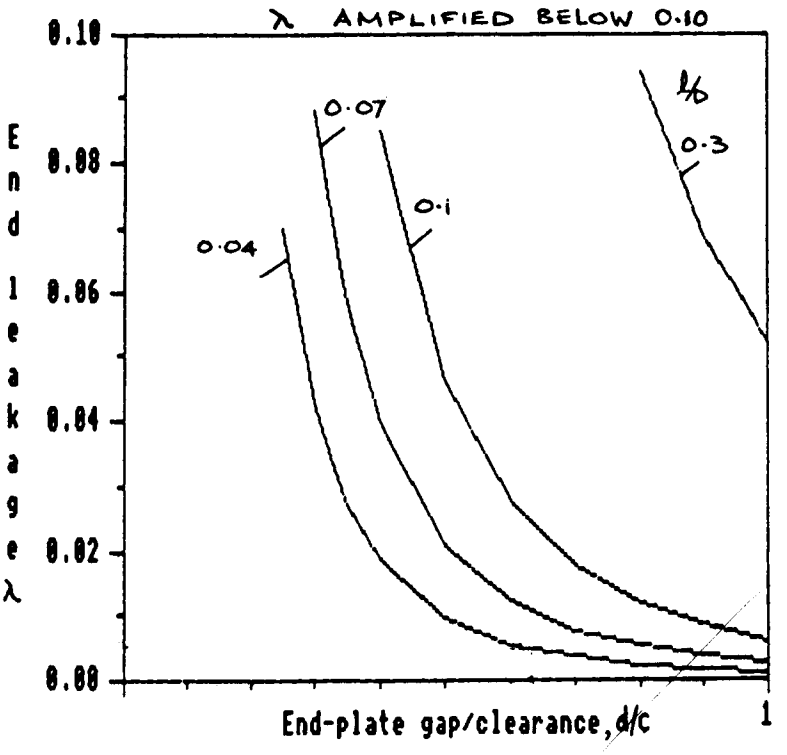

Fig. 7c - λ values for different $\ell_{/D}$ ratios.

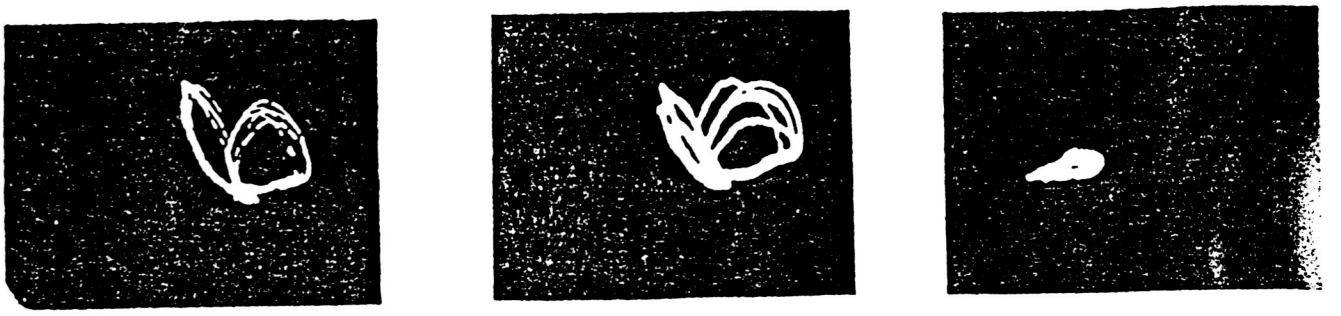

3880 rev/min 4059 rev/min 5075 rev/min

a) Experimentally-observed orbits

3880 rev/min 4059 rev/min 5075 rev/min

b) Numerically-predicted orbits

Fig. 8 : Subharmonic vibrations.

a) experimental b) numerically predicted

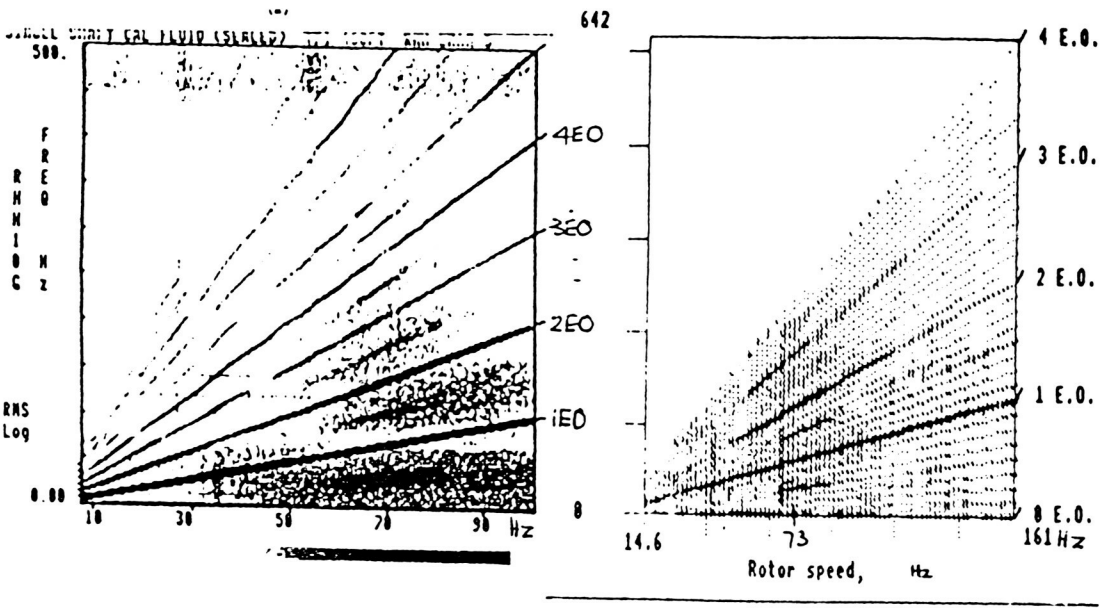

Fig. 9 : z-modulations of horizontal LP rotor vibration relative to the squeeze-film housing.

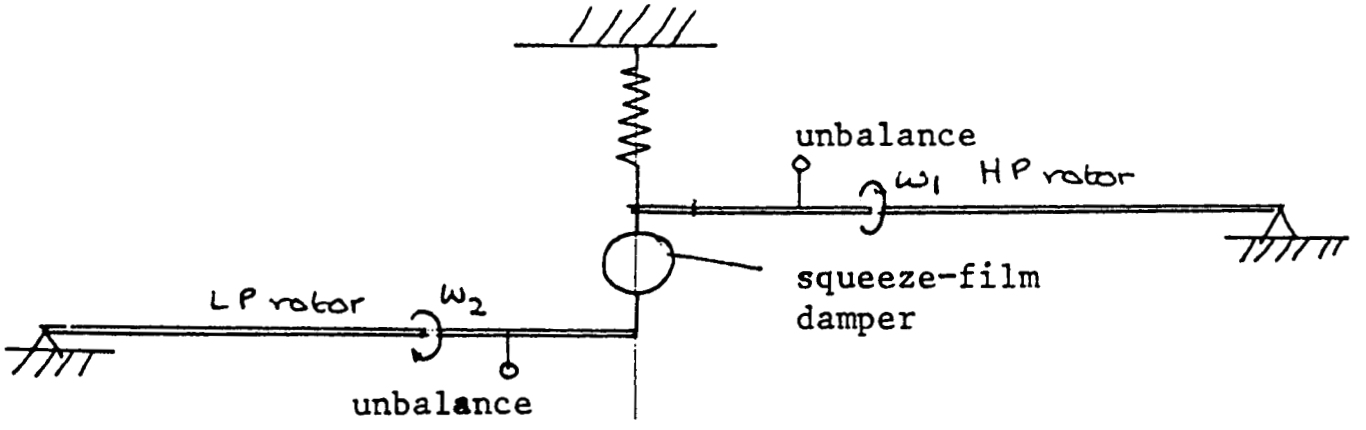

Fig. 10 - Line diagram of test rig.

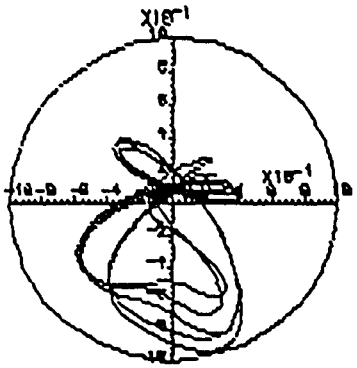

(a)

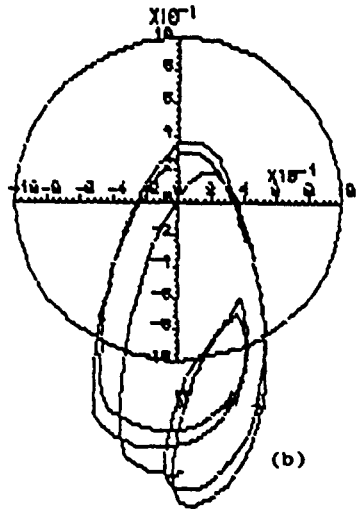

(b)

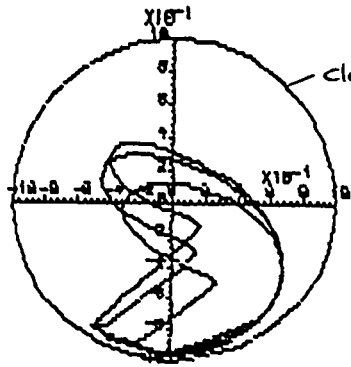

(c)

clearance circle

Fig 11 $\omega_{1,2}$ in same directions.

$\omega_1/\omega_2 = 2$

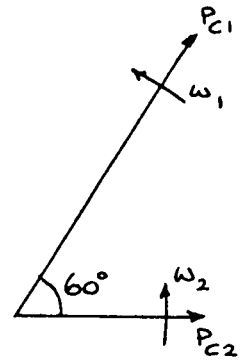

phasing at t = 0

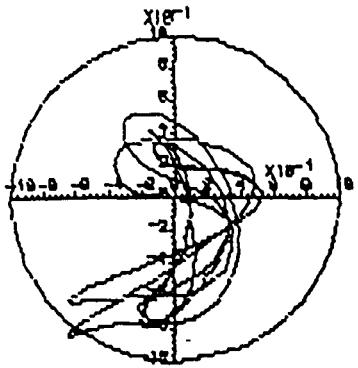

(a)

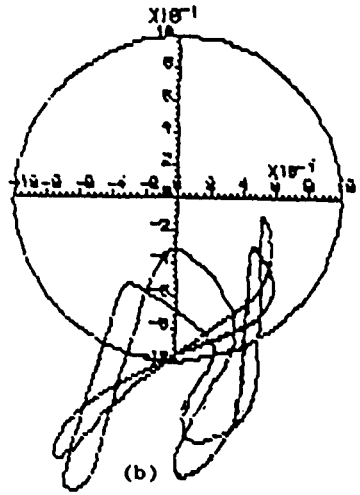

(b)

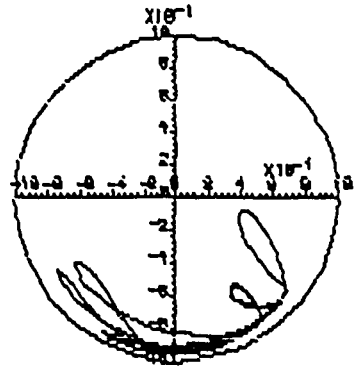

(c)

Fig.12 $\omega_{1,2}$ in opposite directions.

$\omega_1/\omega_2 = 2$

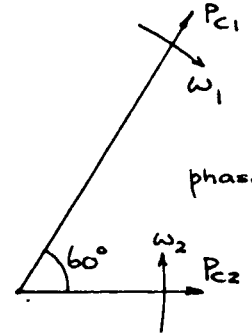

phasing at t=0

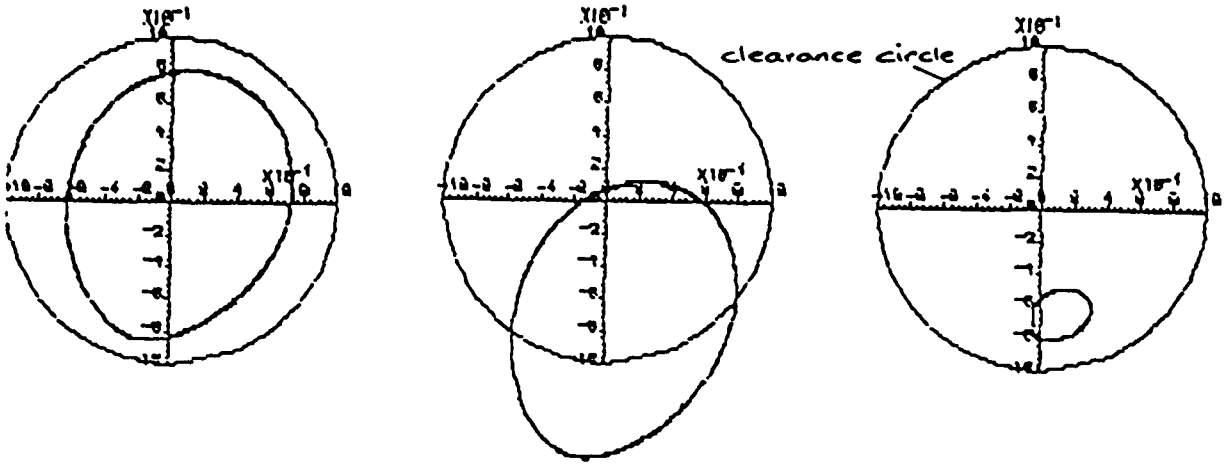

$\omega_{1,2}$ in same directions

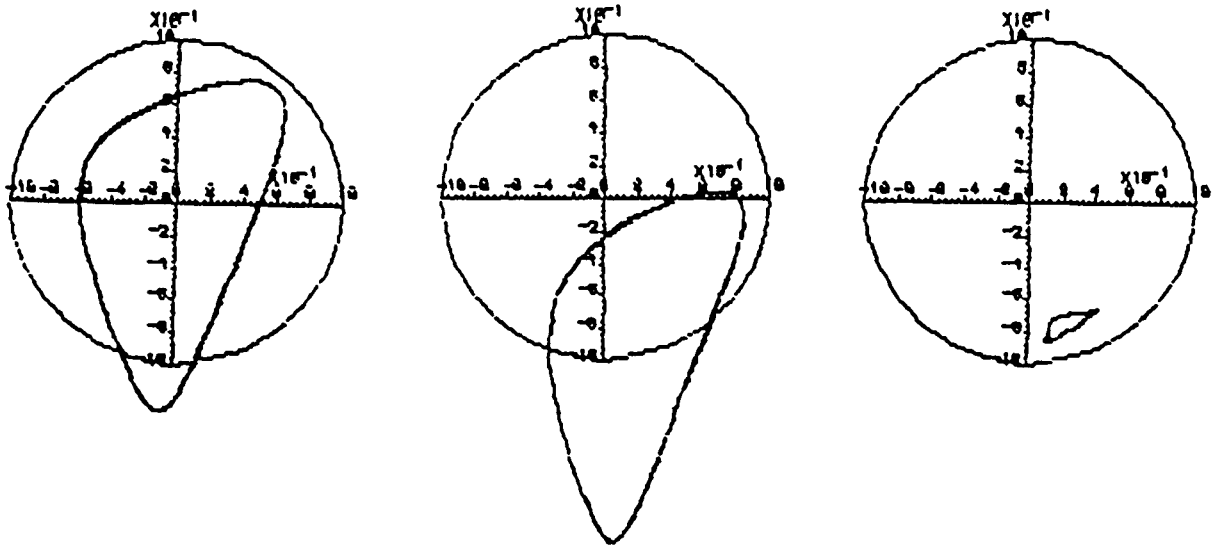

$\omega_{1,2}$ in opposite directions

Fig 3: Vibration orbits for the cases of Figs.5,6 but with end plates $\lambda = 0.1$.

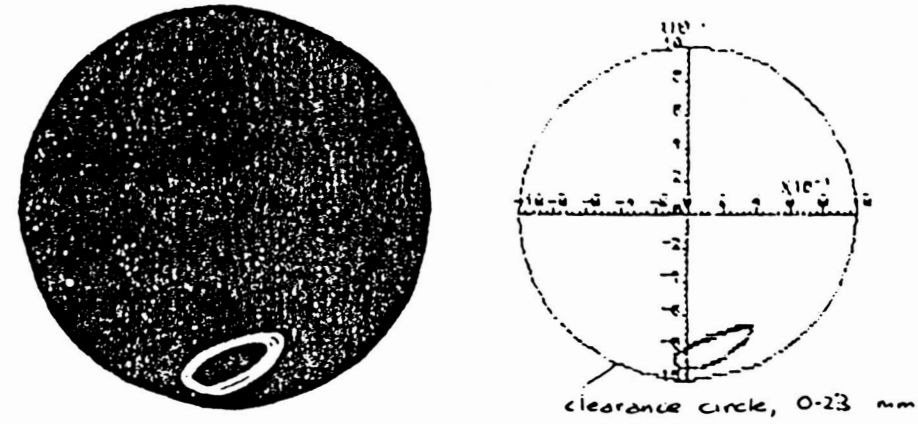

Rotor vibration relative to housing

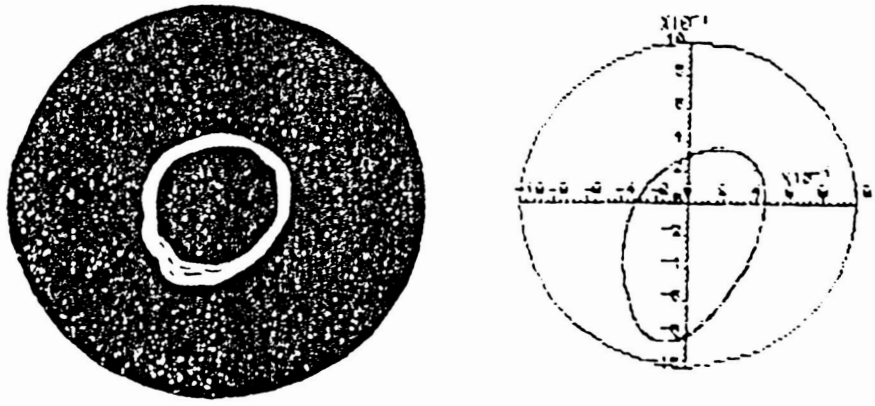

Housing vibration relative to ground

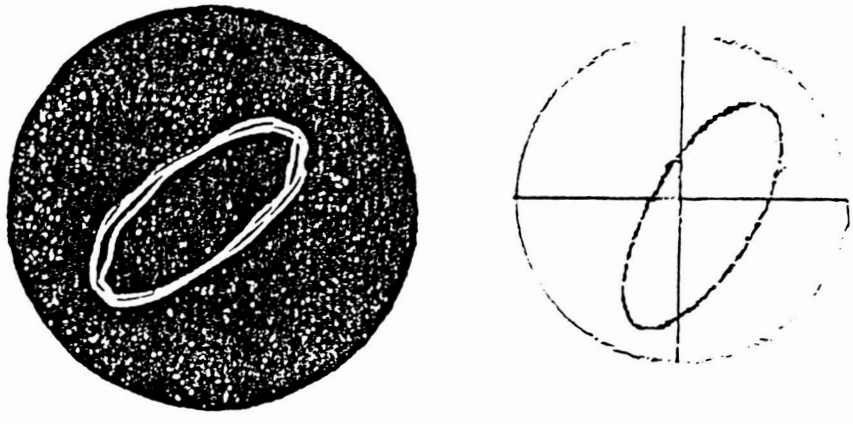

Rotor vibration relative to ground

Fig 14. R10 oil shaft 2 rotating at 3000 rev/min

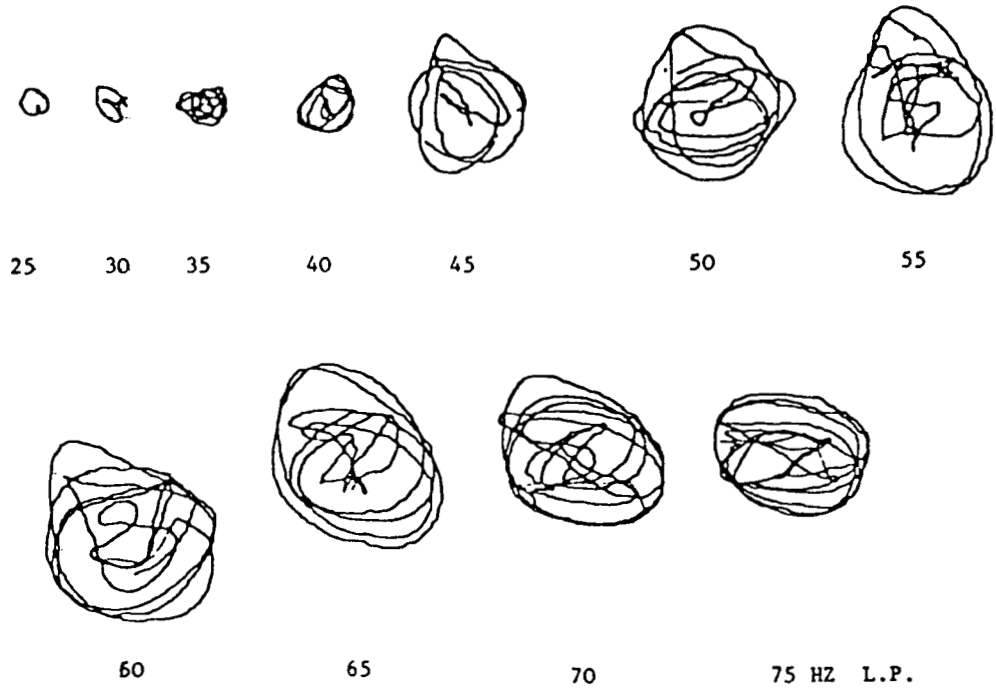

a) Experimental orbits

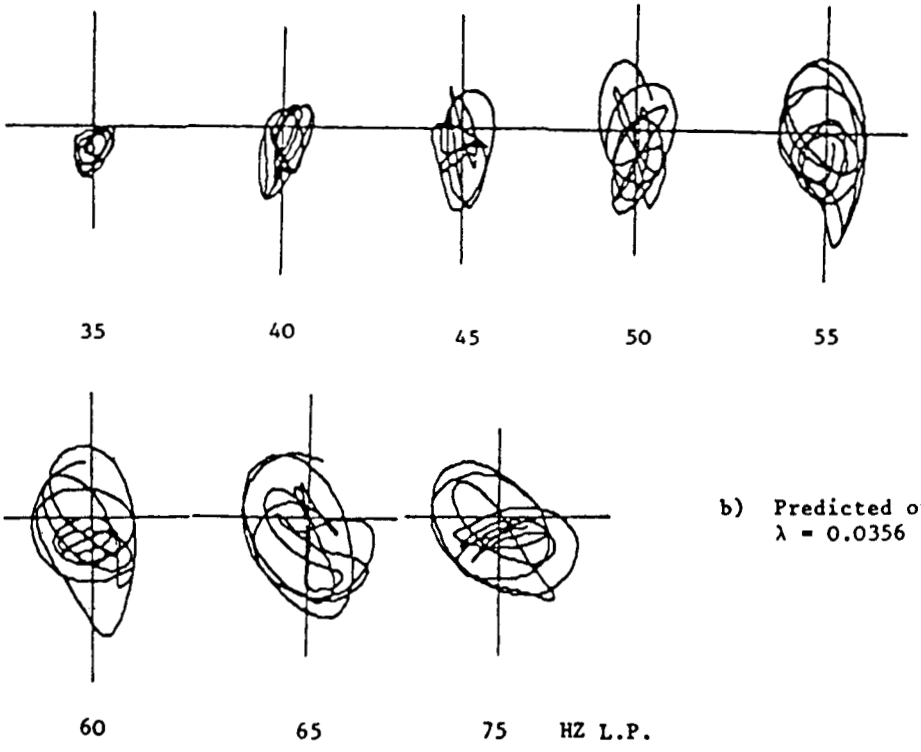

b) Predicted orbits
$\lambda = 0.0356$

Fig. 15 : Experimental and numerically-predicted orbits of rotor vibration relative to ground, co-rotation $\frac{\omega_1}{\omega_2} = +1.3$

scale 1 mm ≡ 1.413 cm

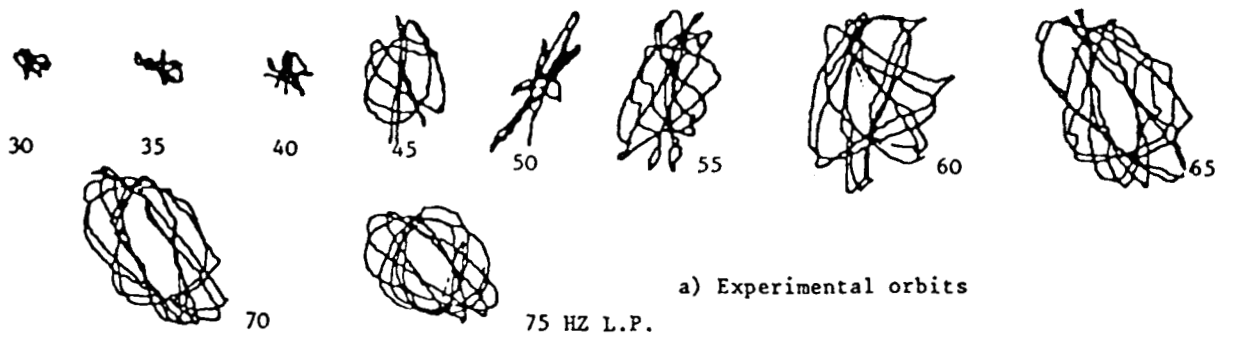

a) Experimental orbits

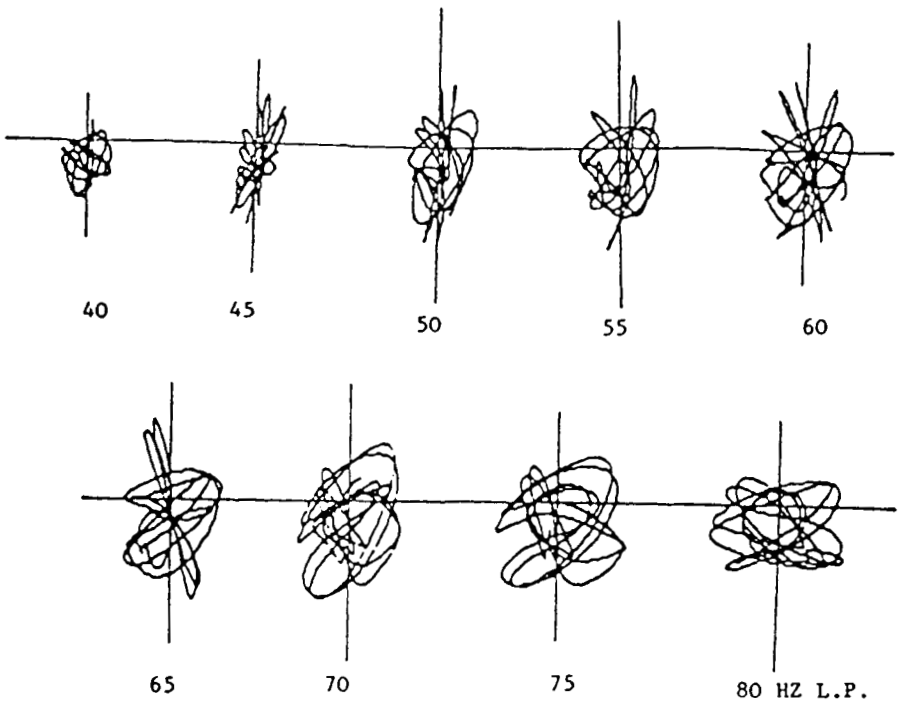

b) predicted orbits , $\lambda = 0.0356$

Fig. 16 : Experimental and numerically-predicted orbits of rotor vibration relative to ground, counter-rotation, $\frac{\omega_1}{\omega_2} = -1.3$

scale 1 mm ≡ 1.413 cm

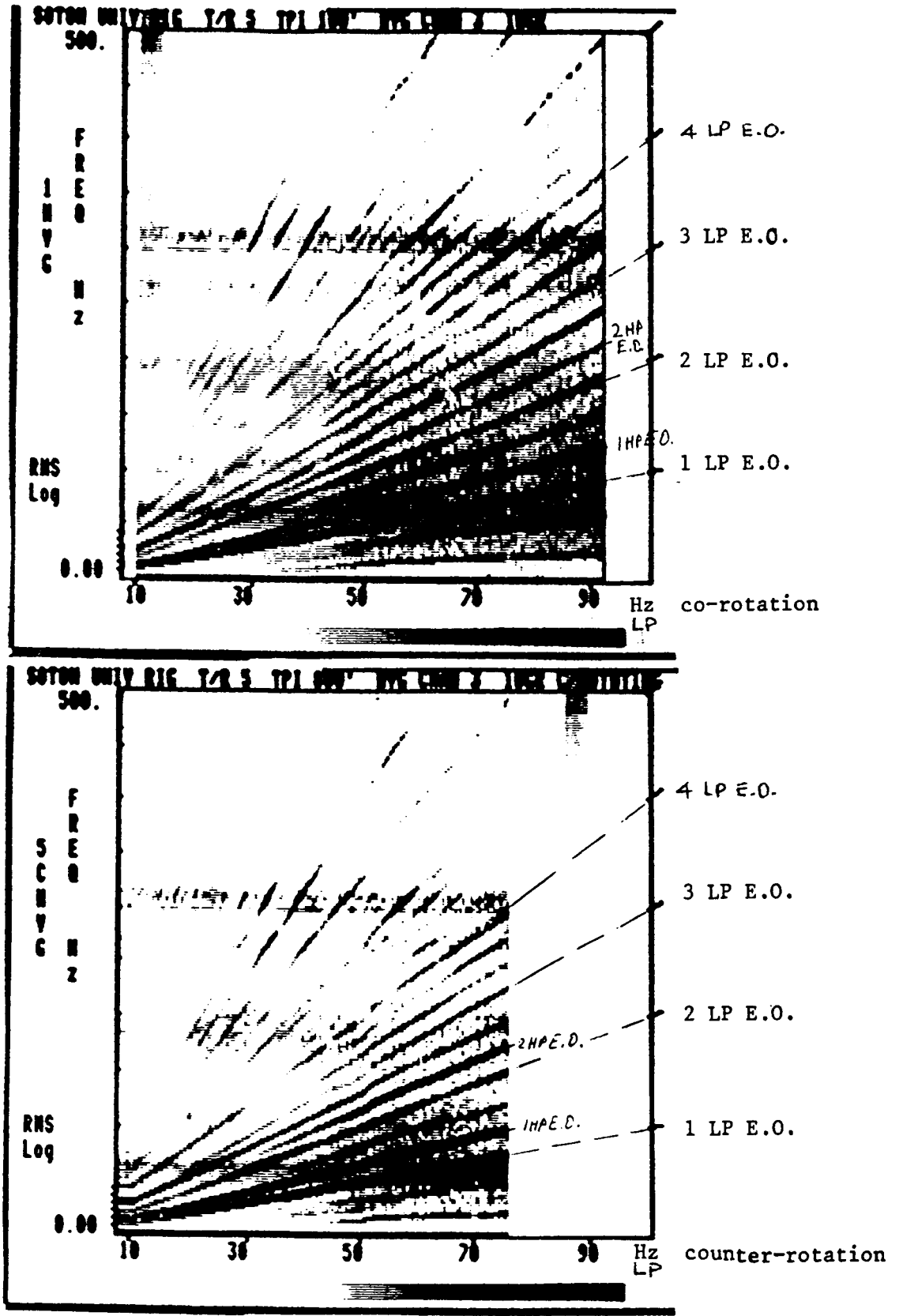

Fig. 17 : z-mods for co-rotation and counter rotation, $\frac{\omega_1}{\omega_2} = \pm 1.3$

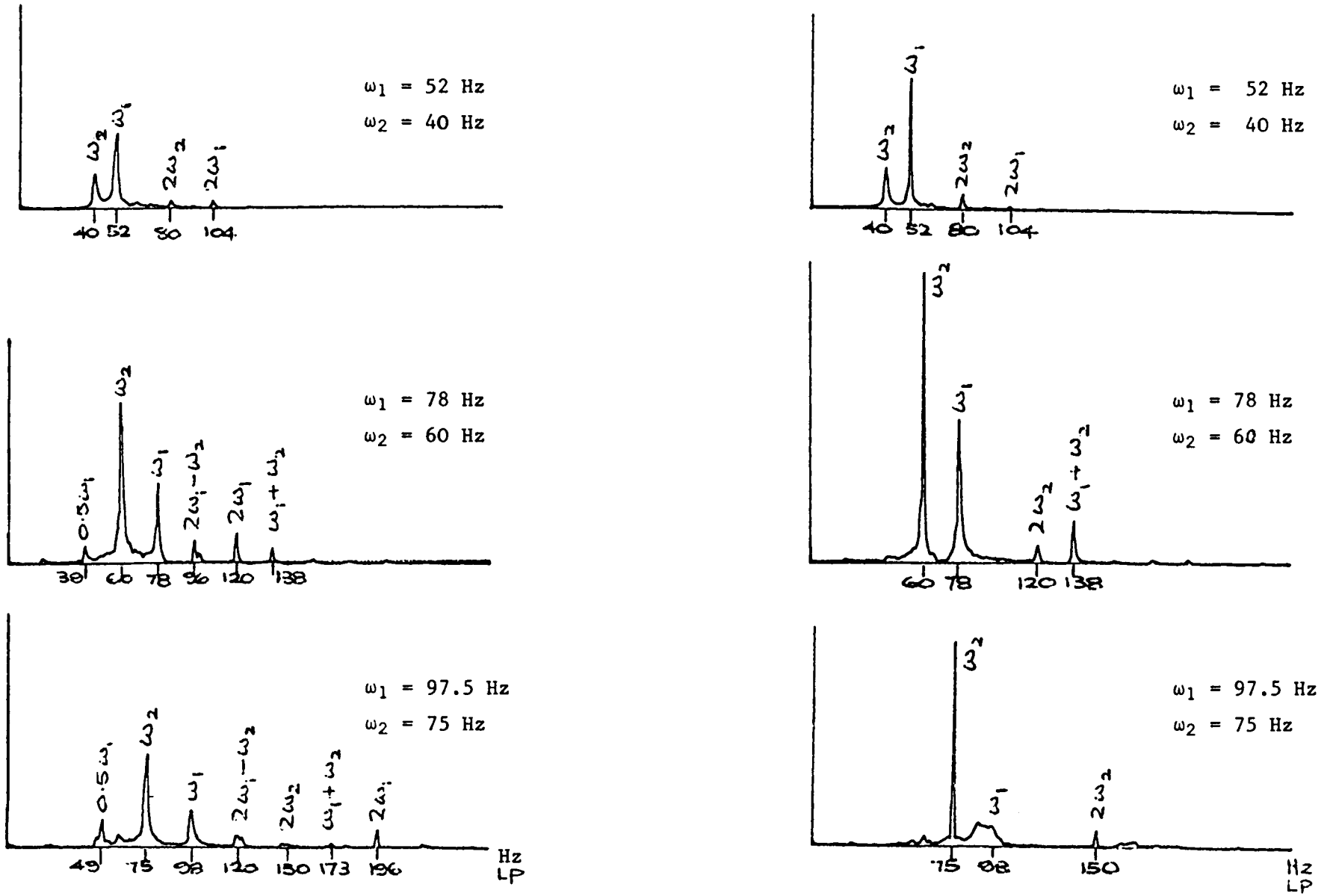

a) co-rotation

b) counter-rotation

Fig. 18 : Frequency spectra.